Journal of Structural Geology, Vol. 14, No. 3, pp. 271 to 280, 1992
Printed in Great Britain

0191-8141/92 $05.00+0.00

Vorticity analysis in a metachert from the Sanbagawa Belt, SW Japan

S. R. WALLIS

Department of Geology and Mineralogy, Faculty of Science, Kyoto University, Kyoto 606, Japan

(*Received* 2 *January* 1991; *accepted in revised form* 16 *August* 1991)

Abstract—Common tectonic features of deformed metachert include both sets of extended and shortened veins and quartz *c*-axis preferred orientation patterns. In such rocks information is also commonly available on the orientation and magnitude of the finite strain. These features can be used to derive two independent estimates of the degree of non-coaxiality during deformation. In an example from the Sanbagawa Belt, SW Japan, the two methods give consistent results and show that deformation was intermediate between simple and pure shear. Such types of progressive deformation distributed over a broad region could cause substantial subvertical thinning and be a significant factor in the exhumation of high *P–T* rocks in the region.

INTRODUCTION

IN THE study of deformation in ductile shear zones the simplifying assumption is commonly made that strain has accumulated by progressive simple shear. However, other types of steady-state progressive deformation are also possible. For deformation with no volume change three types of plane-strain steady deformation can be defined: pure shear, simple shear and general non-coaxial shear that is intermediate between the other two. For these types of deformation the differences in the type of associated flow can be described in terms of the degree of non-coaxiality (Malvern 1969, Elliott 1972, Means *et al.* 1980, Lister & Williams 1983, Passchier 1986). One useful measure of this is the kinematic vorticity number, W_n, where $W_n = 0$ for pure shear, $W_n = 1$ for simple shear (Passchier 1988a,b). Deformation that does not conserve volume can be described in terms of an analogous quantity the kinematic dilatancy number, A, as proposed by Passchier (1991). In this paper I shall largely restrict my discussion to two-dimensional flow types where $A = 0$ (no volume change).

W_n is a measure of the instantaneous degree of non-coaxiality. A quantity W_m can also be defined that is a parameter of finite deformation (Passchier 1988a,b) and expresses the mean value of W_n. For steady-state deformation $W_n = W_m$.

Two of the most important parameters for reconstructing the pre-deformational geometries of domains that have undergone progressive ductile deformation are W_m and the finite strain. There are many methods available for estimating finite strain in rocks (a review of this subject is given by Ramsay & Huber 1983). However, there has been less discussion of methods for quantifying the degree of non-coaxiality.

A number of potential methods for determining the degree of non-coaxiality of deformation have been suggested (Ghosh & Ramberg 1976, Ghosh 1987, Passchier 1988a,b, 1990a) and quantitative studies on the degree of non-coaxiality have used rotated rigid objects (Passchier 1987b, Vissers 1989, Cowan 1990) or the rotation and stretch of material lines (Passchier & Urai 1988). Quartz *c*-axis fabrics have also been used to suggest qualitatively that regions of ductile non-coaxial deformation departed significantly from simple shear (Law *et al.* 1984, Platt & Behrmann 1986, Schmid & Casey 1986).

After a finite period of steady progressive deformation the angular separation of given material lines from fixed elements of the flow field (e.g. instantaneous stretching axes, flow apophyses) is a function of three variables,

(i) the degree of non-coaxiality, W_m;
(ii) the finite strain; and
(iii) volume change.

In metachert the orientation and magnitude of the finite strain ellipsoid can commonly be estimated from the shape of deformed radiolarians. The orientation of fixed elements of flow can be found from sets of shortened and stretched veins and quartz *c*-axis fabrics, and with an estimate of the volume change during deformation these features can be used to estimate W_m. Both quartz *c*-axis fabrics and deformed veins are common elements of the tectonic fabric in deformed metachert, which make it a material well-suited for estimating W_m.

In this paper I use an estimate of the finite strain with the orientation of deformed veins and the quartz *c*-axis fabric to derive two independent estimates for W_m for a sample of metachert.

DESCRIPTION OF FLOW

Instantaneous flow

Instantaneous flow can be described in a continuous medium in terms of the spatial gradients in velocity. These are the components of the velocity gradients tensor, L_{ij} (Malvern 1969, p. 147). L_{ij} can be factored into an instantaneous stretch and an instantaneous rigid-body rotation. The axis of the rigid-body rotation and its

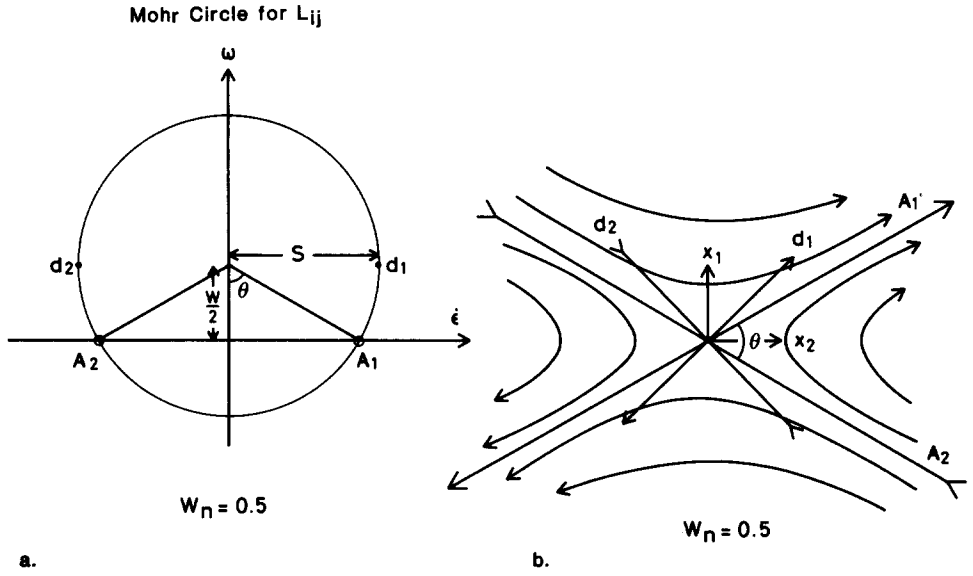

Fig. 1. (a) Mohr space representation of instantaneous two-dimensional flow for $W_n = 0.5$. Any point on the circle represents the instantaneous angular velocity, ω, and stretching rate, $\dot{\varepsilon}$, of a particular material line. W = vorticity; A_i = flow apophyses; d_i = stretching axes of flow. N.B. Material lines instantaneously parallel to these axes have an angular velocity with respect to the flow apophyses and therefore rotate after a finite time; the stretching axes, however, remain fixed with respect to the flow apophyses. (b) Instantaneous flow parameters in real space corresponding to (a); x_i = reference frame; the vorticity vector, **w**, lies perpendicular to the page.

magnitude are described by the vorticity vector, **w** (Malvern 1969, p. 147). In many natural examples of deformation the vorticity vector (parallel to the two-fold axis of quartz *c*-axis fabrics, rotated porphyroclasts, etc.) is subparallel to the intermediate finite strain axis. Under this condition deformation can be analysed in two dimensions in a plane perpendicular to **w**.

Several different measures of the degree of non-coaxiality have been proposed. In this paper I shall use a kinematic vorticity number, W_n, where

$$W_n = W/(s_1 - s_2) \quad \text{(after Passchier 1988a,b).} \quad (1)$$

W is the magnitude of the vorticity vector, and s_1, s_2 are the maximum and minimum rates of stretching. For deformation that conserves volume and with negligible stretch parallel to the vorticity vector W_n is equal to the vorticity number proposed by Truesdell (1954). If reference axes are placed at 45° to the instantaneous stretching axes, d_1 and d_2 (Fig. 1) then for flow that conserves area perpendicular to **w**, $s_1 = -s_2 = S$ and L_{ij} can be written

$$L_{ij} = \begin{bmatrix} 0 & S + W/2 \\ S - W/2 & 0 \end{bmatrix} = \begin{bmatrix} 0 & S + W_nS \\ S - W_nS & 0 \end{bmatrix} \quad (2)$$

(Passchier 1987a). Like any second-order tensor, L_{ij} can be represented by a Mohr circle (Malvern 1969, p. 111, Means 1983). The Mohr circle for L_{ij} and the corresponding flow patterns in real space is shown in Fig. 1 (see also Lister & Williams 1983). The axes are in units of angular velocity, ω, and stretching rate, $\dot{\varepsilon}$. A point on the circle represents the instantaneous stretching rate and angular velocity of a particular material line. The distance from the horizontal axis to the centre of the circle is equal to half the vorticity. In general there will be two material lines that have a zero instantaneous angular velocity. These lines are permanently fixed to two spatial lines termed flow apophyses after Ghosh & Ramberg (1976) and labelled A_i after Passchier (1988b). The two material lines differ in that one is extending and the other shortening. In a three-dimensional symmetrical flow, where the vorticity vector lies normal to the flow apophyses, the extensional apophysis, A_1, and the vorticity vector define a flow plane. The angle between the flow apophyses, θ, is simply related to W_n by

$$\cos\theta = W_n. \quad (3)$$

For simple shear $\theta = 0°$ and for pure shear $\theta = 90°$.

The Mohr circle in Fig. 1 is for instantaneous deformation only. However, for steady-state flow the flow apophyses and the instantaneous stretching axes will not rotate with respect to the reference frame even after a finite time. Material lines will rotate and approach the extensional apophysis but will not cross it. For equal-area deformation the rotation of particular material lines, e.g. parallel to the finite strain axes, depends on two factors, W_n and the finite strain. The next section will show how these factors are related.

Finite deformation

The position gradients tensor, F_{ij} (also referred to as the deformation gradients tensor, e.g. Malvern 1969, p. 156), operates on an infinitesimal material vector to associate it with a new vector in the deformed state. The inverse of F_{ij} is referred to as H_{ij} and relates particle positions in the deformed state back to the original undeformed state. F_{ij} can be derived for steady flow by integration of L_{ij} over a finite time interval. The eigenvectors of the symmetrical part of F_{ij} represent the principal axes of the strain ellipsoid. However unlike the

strain tensor, F_{ij} also contains information about the rotational component of finite deformation.
F_{ij} can be written:

$0 < W_n < 1$

$$F_{ij} = \begin{bmatrix} \cosh\{\sqrt{(1-W_n^2)}\cdot St\} & \frac{(1+W_n)}{\sqrt{(1-W_n^2)}}\sinh\{\sqrt{(1-W_n^2)}\cdot St\} \\ \frac{(1-W_n)}{\sqrt{(1-W_n^2)}}\sinh\{\sqrt{(1-W_n^2)}\cdot St\} & \cosh\{\sqrt{(1-W_n^2)}\cdot St\} \end{bmatrix} \quad (4)$$

$W_n = 1$

$$F_{ij} = \begin{bmatrix} 1 & 2St \\ 0 & 1 \end{bmatrix} \quad (5)$$

(MacKenzie 1979, Passchier 1988a,b). These equations must be modified if deformation involves a change in area (Passchier 1988a,b, 1990a). The magnitude and orientation of the principal axes of strain can be determined from the components of F_{ij}. The finite strain ratio is given by:

$$R_f = (F_{11}^2 + F_{12}^2 + F_{21}^2 + F_{22}^2)/2 + [(F_{11}^2 + F_{12}^2 + F_{21}^2 + F_{22}^2)^2 - 1]^{1/2}, \quad (6)$$

and the orientation with respect to the reference frame from:

$$\tan 2\Omega = \frac{2(F_{11}^2 + F_{12}^2 + F_{21}^2 + F_{22}^2)}{(F_{11}^2 - F_{12}^2 + F_{21}^2 - F_{22}^2)} \quad (7)$$

MacKenzie (1979).

Alternatively calculations can be performed by representing F_{ij} as an off-axis Mohr circle in stretch space (Means 1982, Bobyarchick 1986, Passchier 1988a,b). Steady-state accumulation of strain is represented by a series of circles with increasing radii (Fig. 2). The centre of the circle shifts during deformation and follows a path that is dependent on W_n. The orientations of the flow apophyses and the instantaneous stretching axes for every instant of deformation remains constant with respect to the reference frame. This Mohr circle has a number of properties that I shall use in the following analysis.

The circle is plotted in stretch space and the polar co-ordinates of any point on the circle represent the stretch and rotation of a particular material line (Means 1982). The angles within the Mohr circle for F_{ij} refer to the undeformed state. The angle between lines in the deformed state cannot be read directly from this Mohr construction but can be calculated from the original angle and the difference between the amounts of rotation of the two lines. The position and size of the circle can be defined by three quantities R, T and Q (Fig. 2). For two-dimensional deformation that conserves area the radius of the Mohr circle, R, is half the difference between the maximum and minimum stretches, which can be expressed in terms of the ellipticity of the strain ellipse as:

$$R = \tfrac{1}{2}(R_f^{1/2} - R_f^{-1/2}) \quad \text{(Passchier 1988a,b).} \quad (8)$$

The distance of the centre of the circle from the origin, T, is the average stretch and is given by:

$$T = \tfrac{1}{2}(R_f^{1/2} + R_f^{-1/2}) \quad \text{(Passchier 1988a,b).} \quad (9)$$

T and R can also be modified to take into account changes in area during deformation (Passchier 1988a,b, 1990a). For $A = 0$ two of the parameters needed to construct the Mohr circle, R and T, are defined by the finite strain. The third parameter is the distance of the centre of the circle from the horizontal axis, Q (Fig. 2). This distance can be defined in terms of the angle through which the material line now parallel to the axis of maximum finite extension has rotated with respect to the reference frame, ϕ, by the equation,

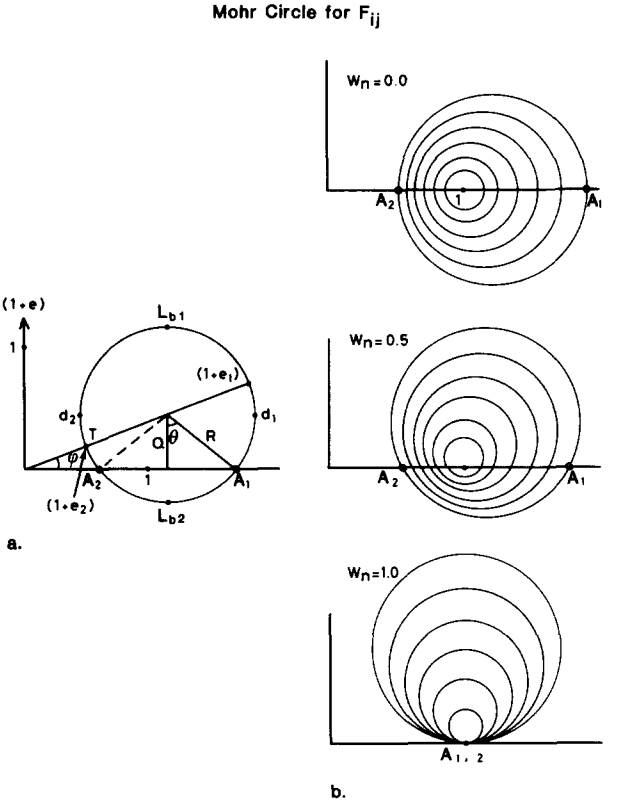

Fig. 2. (a) Mohr circle for F_{ij} representing finite deformation in stretch space. The polar co-ordinates of a point on the circle give the stretch and rotation of a material line. The size and position of the circle can be defined by three parameters: the distance of the centre of the circle from the origin (T); the radius of the circle (R); and the distance of the centre of the circle from the horizontal axis (Q). The principal axes of finite strain lie on a diameter that makes an angle ϕ with the horizontal axis. Lines of zero finite rotation are located at the intersection of the circle with the horizontal axis. These lines are parallel to the flow apophyses, A_i, at every instant for steady flow. Material lines parallel to the instantaneous stretching axes (d_i) and the axes of no instantaneous longitudinal strain at the beginning of deformation (L_{bi}) lie on diameters parallel to the horizontal and vertical axes, respectively. (b) Progressive deformation at a fixed value of W_n can be represented by a series of Mohr circles for F_{ij} with progressively increasing diameters. The angle between A_1 and A_2 remains fixed. The values of R and T increase according to equations (8) and (9). Three series of circles are shown for progressive steady deformation with values of W_n = 0.0, 0.5 and 1.0.

$$Q = T \sin \phi \quad \text{(Fig. 2).} \qquad (10)$$

The mean vorticity number is related to these parameters by the equation,

$$W_m = Q/R \quad \text{(Passchier 1988a,b).} \qquad (11)$$

An analogous treatment of finite deformation is possible using Mohr circles for the reciprocal stretch tensor, H_{ij} (Passchier 1990a,b, Treagus 1990).

The above relationships are used to construct various Mohr circles from fabric elements in metachert samples. These allow limits to be placed on the degree of non-coaxiality of the deformation.

SAMPLE DESCRIPTION

Several samples of deformed metachert were collected from the southernmost part of the Sanbagawa Belt in SW Japan (Wallis & Banno 1990) where it is associated with metabasic material. Fine-grained lawsonite has been reported from metapelite at slightly deeper structural levels (Watanabe & Kobayashi 1984). The chert consists of quartz layers up to 5 mm thick separated by very thin layers of finely disseminated opaques and a small amount of epidote.

The chert is lineated and has a foliation subparallel to bedding. In thin section the mesoscopic lineation can be seen to coincide with both a crenulation and a stretching lineation. The stretching is defined by the elongation of individual quartz grains and deformed radiolarians (Fig. 3a). However a secondary oblique grain-shape fabric is locally well developed, and on average makes an angle of 10° with the main foliation. Similar fabrics have been described elsewhere in quartz-rich tectonites that have undergone non-coaxial deformation (e.g. Law *et al.* 1986). The sense of obliquity of the fabric suggests a top-to-the-east sense of shear. The deformed radiolarians are good strain markers (e.g. Toriumi 1982). The average grain size of the quartz in the matrix is approximately 30 μm. The radiolarians consist of an aggregate of slightly coarser-grained quartz (60–100 μm). The quartz has an undulose extinction and sutured grain boundaries indicative of deformation by intracrystalline plastic processes (Bell & Etheridge 1973, White 1976). Epidote is fractured and pulled apart in the direction of stretching showing that a large part of the ductile deformation took place after the main growth of metamorphic minerals (Fig. 3b).

The foliation is cut by numerous quartz veins and both boudinaged and folded veins are present. The axial planes of the folds are subparallel to the foliation. In thin section the quartz grains within the veins are commonly flattened and stretched parallel to the grains in the matrix. Quartz fibres are locally preserved within the veins, however, they show strong undulose extinction and cannot be used to determine the orientation of the instantaneous stretching axes. These observations show that the veins formed during or before the main ductile features of the sample. Shortened veins typically have an arc-length to thickness ratio <8, which suggests there was a low viscosity contrast between the veins and the matrix. Shortening of the veins was therefore probably accommodated by thickening as well as folding. Stylolites are locally present oriented roughly parallel to the foliation and these probably represent the source for the vein-fill material.

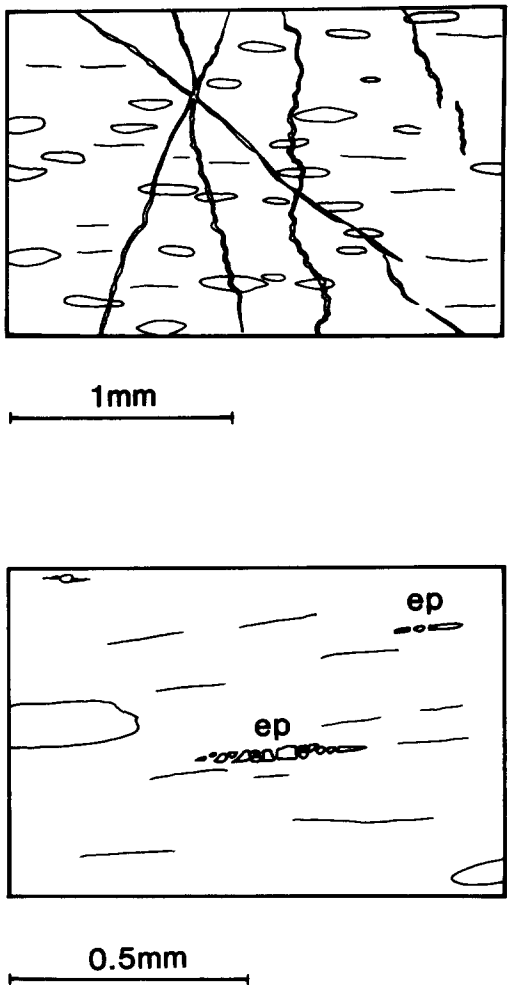

Fig. 3. Sketches from photomicrographs parallel to stretching direction of the metachert sample, MB4. (a) Deformed quartz veins and the outlines of deformed radiolarians are shown. Narrow lines are layers of fine-grained opaques parallel to the foliation. (b) Pull-apart fracturing of epidote (ep) parallel to the stretching lineation shows that the main deformation took place after the peak metamorphism.

PRACTICAL DETERMINATION OF W_m

Finite strain

Finite strain was estimated from the shape of deformed radiolarians using an R_f/ϕ plot and the net designed by De Paor (1988). Three thin sections were made from mutually perpendicular sections: (i) perpendicular to the stretching lineation; (ii) parallel to the lineation and perpendicular to the foliation; and (iii) parallel to foliation. The results show that within the accuracy of measurement the maximum and minimum principal axes of finite strain coincide with the mesoscopic fabric elements of lineation and normal to the

foliation. The results give a strain ratio of $X/Z = 3.4$–3.6 ($=R_f$) and $Y/Z = 1.6$–1.7 (95% confidence limits), which deviates slightly from plane strain and lies in the constrictional field (Fig. 4). This slight deviation away from plane strain may explain the formation of the microcrenulations approximately parallel to the stretching lineation.

The finite strain can be combined with the quartz *c*-axis fabric to estimate W_m (see later). It is also important in the analysis of deformed veins for helping to constrain the possible values for W_m and A. The distribution of deformed veins is studied first because this allows a test of the assumption that deformation was not associated with significant area change in the plane perpendicular to the vorticity vector.

Distribution of deformed veins

During progressive deformation material lines will rotate towards the extensional apophysis. During this rotation the lines may undergo both shortening and extension. Material line markers such as deformed veins and dykes have been used for strain analysis (Talbot 1970) and a qualitative assessment of the non-coaxiality of deformation (Hutton 1982, Passchier 1986). Passchier (1990a) has further shown that it is sufficient to know the orientation of the boundaries between domains of material lines with different stretch histories to determine all the parameters of finite deformation, i.e. W_m, sense of vorticity, finite strain and volume change. In most cases the orientation of material lines can be measured with a high degree of accuracy which makes this a potentially very useful technique for kinematic analyses.

The boundaries between material line sectors with different stretch histories correspond to the orientation of material lines that lie parallel to the lines of no instantaneous longitudinal strain at the onset of deformation and at the final increment of deformation (Passchier 1990a,b). These four lines are labelled L_{ai} and L_{bi} after Passchier (1990a). The subscripts 'a' and 'b' refer to 'after' and 'before' deformation.

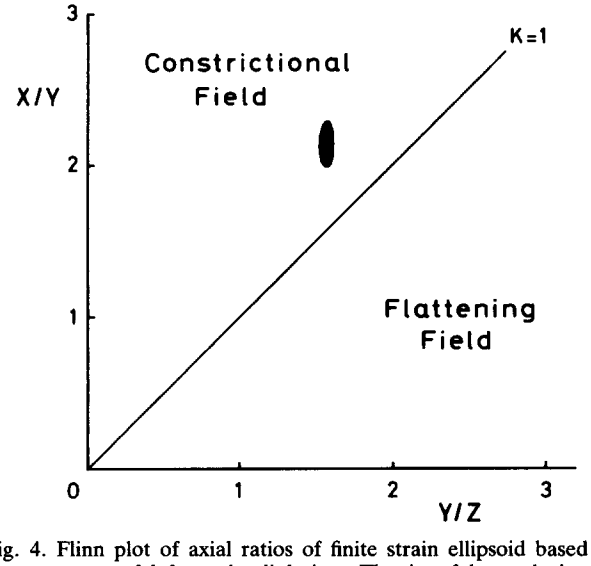

Fig. 4. Flinn plot of axial ratios of finite strain ellipsoid based on measurements of deformed radiolarians. The size of the mark gives an estimate of the two standard deviation error. Finite strain deviates slightly from plane strain in this sample and lies in the constrictional field, with $R_f = 3.4$–3.6.

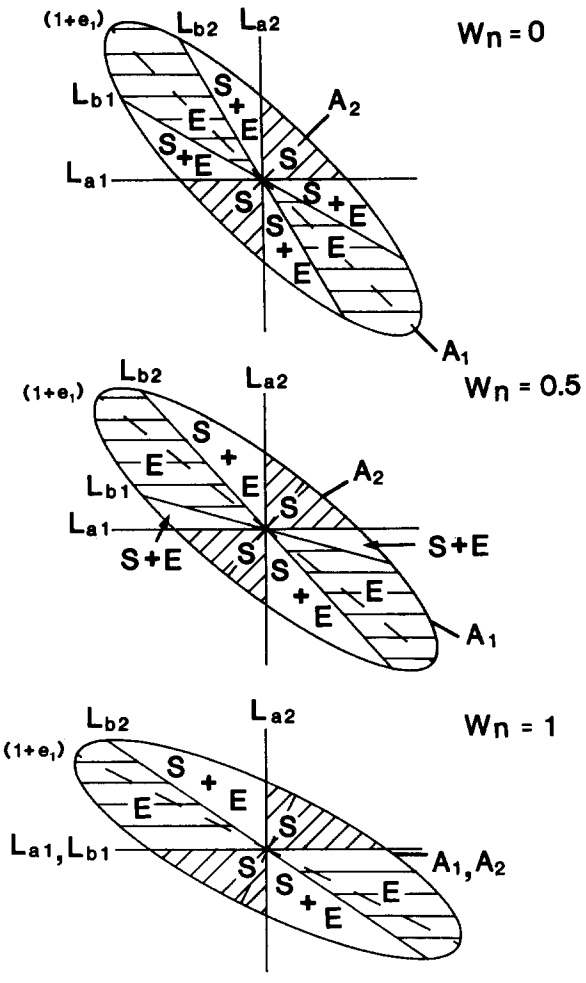

Fig. 5. Three diagrams illustrating the effect of W_n on the distribution of sectors of material lines with different stretch histories. These diagrams are for three types of steady flow with $W_m = W_n = 0.0$, 0.5 and 1.0; $R_f = 3.5$; and $A = 0$. These diagrams are drawn with respect to the lines of zero instantaneous shortening during the final increment of deformation, L_{ai}. $(1 + e_1)$ = maximum finite extension axis, L_{bi} = position after deformation of the material lines that were initially parallel to lines of zero instantaneous shortening. S = shortened lines, S + E = shortened and extended lines, E = extended lines. The position of the lines of zero instantaneous rotation or flow apophyses, A_i, are also shown.

The influence of the degree of non-coaxiality on the distribution of sectors of material lines with distinct stretch histories can be illustrated by considering three different types of two-dimensional equal-area deformation (Fig. 5). The boundary between material lines that have only undergone shortening and those that have undergone shortening followed by extension is the material line that is parallel to the lines of no instantaneous longitudinal strain during the final increment of deformation, L_{ai}. The boundaries between lines with a history of shortening followed by extension and those which have only experienced extension lies parallel to L_{bi} (Passchier 1990a,b). L_{bi} progressively rotates away from L_{ai} with increasing strain up to a value that is a function of the degree of non-coaxiality. During pro-

gressive pure shear, i.e. $W_n = 0$, L_{bi} will rotate symmetrically towards the extension direction. In contrast during progressive simple shear, i.e. $W_n = 1$, L_{b1} is fixed to the shear plane while L_{b2} progressively rotates. This produces a strong asymmetry in the sectors with distinct stretch histories (Fig. 5). For intermediate types of progressive deformation, $0 < W_n < 1$ the distribution of sectors with different stretch histories is asymmetric and intermediate between pure and simple shear. The orientations of these boundaries are a function of W_n and finite strain (Fig. 5).

Deformed veins of the metachert samples were measured in a section perpendicular to the Y axis of the strain ellipsoid. This direction is parallel to the two-fold axis of the quartz c-axis fabric (see later) and therefore also parallel to the vorticity vector. The veins can be separated into those which have only been shortened; those which have undergone shortening followed by extension; and those which only show indications of extension (Fig. 6). However, the distribution of sets of deformed veins will not exactly correspond to sectors of material lines with different stretch histories (Talbot 1970, Passchier 1990a). Veins that passed from the shortening to the extensional field may first begin to unfold before showing any signs of necking or boudinage and veins that have first been shortened may completely unfold so no evidence remains of the earlier shortening history. Unfolding is likely to be most complete when there is a high competency contrast between the vein and matrix materials. In the sample material geometries of folded veins suggest a very low competency contrast between matrix and vein material (see above) and the effect of unfolding is, therefore, likely to be minimal.

A plot of the distribution of deformed veins has an asymmetric distribution of vein sectors (Fig. 6) that indicates a top-to-the-east sense of shear, which is consistent with the microstructural evidence. The boundary between veins that have been shortened only and those that have been shortened and then extended can be defined to within a few degrees. If the effect of unfolding is small (a few degrees) then these boundaries will lie close to L_{b1} and L_{b2}, the two lines of zero instantaneous shortening during the final increment of deformation.

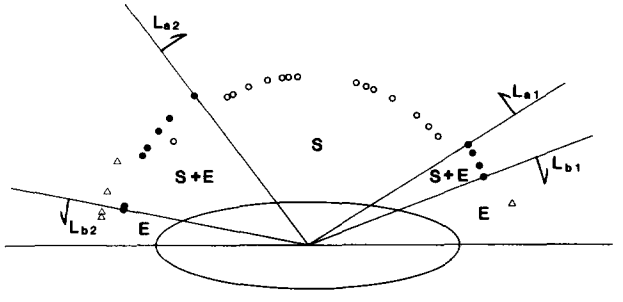

Fig. 6. Distribution of deformed veins in the metachert. The data are compiled from three separate samples. Open circles = shortened veins, black dots = shortened and extended veins, open triangles = extended veins. The distribution of veins with different stretch histories places constraints on the possible location of L_{ai} and L_{bi}. The data are plotted with respect to the foliation. An ellipse of $R_f = 3.5$ shows the estimated finite strain in the matrix.

Observation agrees closely with the prediction that for deformation with no area change these boundaries should be perpendicular (Fig. 6). Some veins that only show evidence for extension plot in the field where other veins have undergone an earlier phase of shortening. This is probably because a certain amount of initial shortening will be accommodated by thickening of the veins which is not easily recognized.

Although the orientations of L_{ai} and L_{bi} cannot be directly determined from the vein arrays, limits can be placed on their orientations. In this sample there is also a limit on the possible finite strain that the deformed veins represent. The limits on the orientations of L_{ai}, L_{bi} and the finite strain are:

$$L_{a1} \wedge L_{a2} < 95°,$$
$$L_{b1} \wedge L_{b2} < 32°$$

and

$$R_f < 3.6.$$

There is also a degree of uncertainty in the orientation of L_{ai} with respect to L_{bi}, which depends on the angles taken for $L_{a1} \wedge L_{a2}$ and $L_{b1} \wedge L_{b2}$. With the above values a range of possible Mohr circles for F_{ij} or H_{ij} can be constructed following the procedure described in Passchier (1990a). These circles give upper and lower limits for the parameters of finite deformation, i.e. A, W_m, R_f.

Some of the constraints can be illustrated using Mohr circles for the maximum strain estimated in the sample, $R_f = 3.6$, and zero area change, $A = 0$ (Fig. 7). The angle between $L_{a1} \wedge L_{a2}$ is simply related to A, the kinematic dilatancy number by the equation,

$$\cos(L_{a1} \wedge L_{a2}) = A \quad \text{(Passchier 1990a, 1991).}$$

An angular separation of $L_{a1} \wedge L_{a2}$ less than 90° implies an area increase. The data from the deformed vein sets give an upper limit of $L_{a1} \wedge L_{a2} < 95°$ for the sample. A lower limit can also be found using the constraints imposed by the finite strain and the orientation of the extensional veins. The Mohr circles in Fig. 7 are drawn for $A = 0$ and $R_f = 3.6$. Any increase in $L_{a1} \wedge L_{a2}$ requires a finite strain greater than that measured in the sample to account for the relatively narrow extensional sector. A decrease in the extensional sector, $L_{b1} \wedge L_{b2}$, is likewise only possible for higher finite strain. This therefore implies a lower limit of $L_{a1} \wedge L_{a2} > 90°$. The range of possible origins shown in Fig. 7 stems from the uncertainty about the orientation of L_{ai} with respect to L_{bi}. A second set of Mohr circles can be plotted that include the possibility of a small amount of area decrease.

From the above analysis the ranges of possible values of the deformation parameters are:

$$0 < A < -0.09,$$
$$0.51 < W_m < 0.70$$
$$3.4 < R_f < 3.6.$$

The angle between the horizontal axis and the centre of the Mohr circle in Fig. 7, ϕ, ranges from 17° to 24°. This

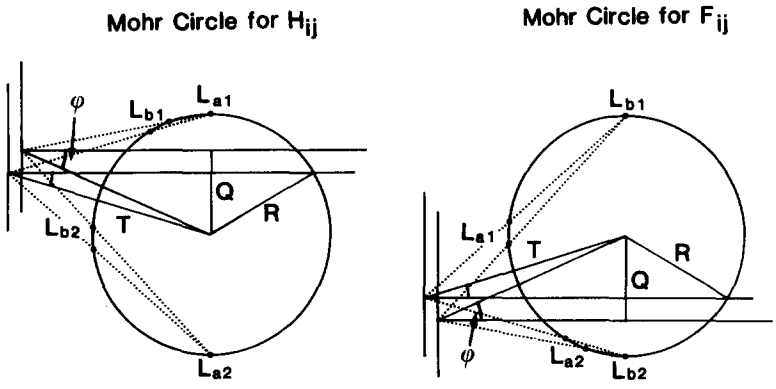

Fig. 7. A range of possible Mohr circles for equal area deformation determined from the distribution of deformed veins. The plotting technique follows Passchier (1990a). Mohr circles for both the stretch tensor, F_{ij}, and the reciprocal stretch tensor, H_{ij}, are shown. These circles are plotted using the maximum estimate of finite strain: $R_f = 3.6$. The angle between $L_{a1} \wedge L_{a2}$ is set at 90° (180° in Mohr space) implying no area change. This is a lower limit for the sample because any decrease in this angle, i.e. an area increase, requires a higher finite strain than that measured. An upper limit of 95° for $L_{a1} \wedge L_{a2}$ is given by the deformed vein sets (Fig. 6). Other Mohr circles can be drawn including this small degree of area loss, however, the maximum and minimum estimates for W_m are derived if the area change is zero. The parameters of the Mohr circles shown in this figure are therefore, $R_f = 3.6$, $A = 0$, $0.51 < W_m < 0.70$. The angle ϕ is used later to compare these results with the quartz *c*-axis data; $17° < \phi < 24°$. N.B. The estimate of finite strain from deformed radiolarians suggests a minor departure from plane strain in the constrictional field. Finite strain with $Y < 1$ causes an area increase in the X–Z plane. However, the analysis of deformed veins constrains the area change in this plane to be less than or equal to zero. These two observations imply deformation included small amounts of both constrictional strain and volume decrease. This has no effect on the estimates of W_m.

is used later to compare with the estimate of W_m from the quartz *c*-axis fabric.

The results of this analysis show that deformation was not associated with any significant area change in the plane of analysis (less than 1%). The finite strain estimated from the deformed veins has the same range as that estimated from the matrix. This suggests the veins (and stylolites) formed before the onset of ductile deformation and suffered the same deformation as the matrix. In all cases deformation is non-coaxial and shows a significant departure from simple shear.

Quartz c-axis fabrics

The metachert has a strong crystallographic preferred orientation (Fig. 8). The asymmetry in both topology and density distribution with respect to the foliation suggests a top-to-the-east sense of shear. This fabric was contoured and the fabric skeleton drawn for the central part of the diagram (Fig. 8).

The modelling of Lister & Hobbs (1980) predicts that the central girdle of quartz *c*-axis diagrams develops perpendicular to the flow plane in both simple and pure shear. This prediction is supported by the work of Law *et al.* (1990). Platt & Behrmann (1986) suggested that the central girdle will also form perpendicular to the flow plane during general non-coaxial deformation and the flow path modelling of Vissers (1989) supports this proposition. Under this assumption the angle between the perpendicular to the central girdle and the foliation is equal to the angle between the flow plane and the flattening plane of strain, β. For $A = 0$ this angle is a function of W_n and the finite strain only. In this sample β is estimated to be 5–8° (Fig. 8) and can be plotted on a Mohr circle as the angle ACB as shown in Fig. 9. The angle ACB can be shown to be equal to β by the following reasoning. Let α be the angle between the flow apophysis, A_1, and the line in the *undeformed* state that is now parallel to the line of maximum elongation. This angle is equal to β plus the rotation of the flattening plane ϕ (Fig. 9). In Fig. 9, α is the sum of the two acute angles BAC and ACB. BAC is defined as ϕ therefore ACB must be equal to β.

For deformation that conserves area the finite strain defines two of the parameters of the Mohr circle, i.e. its radius R and the distance of the centre from the origin T

$R = 0.65$–0.69 from equation (8)

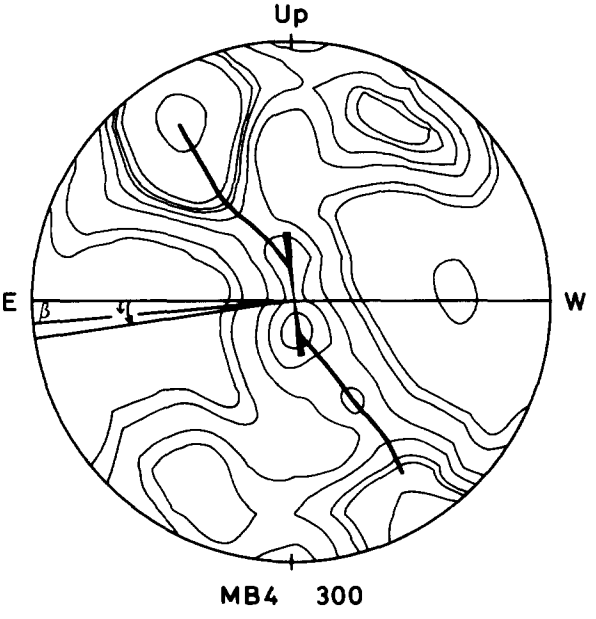

Fig. 8. Quartz *c*-axis fabric measured in the metachert based on 300 measurements. Contoured at equal probability levels with an algorithm of Fisher and Dingle (Fisher *et al.* 1987). The fabric skeleton is drawn by joining up the peaks along crest lines (Lister & Williams 1979). The angle between the normal to the central part of the fabric skeleton and the foliation is β, with $5° > \beta > 8°$.

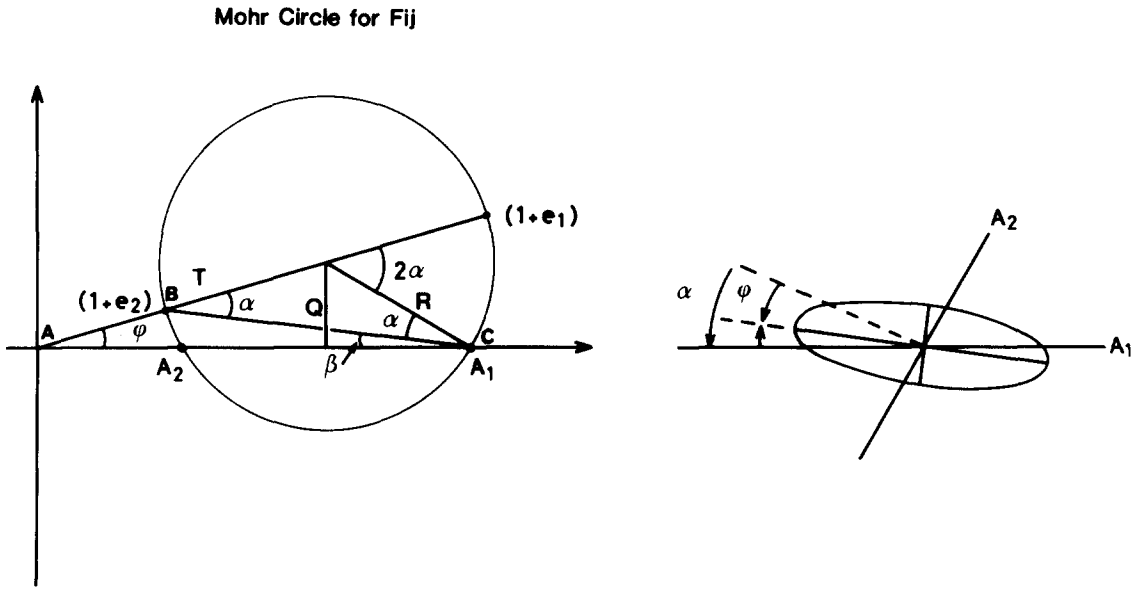

Fig. 9. (a) Plot of the angle between the flow plane and axes of finite strain (β) on the Mohr circle for F_{ij} in stretch space. T = the distance from the origin to the centre of the circle, Q = the distance of the centre of the circle above the horizontal axis, R = the radius of the circle. See text for discussion of the relationship between β, ϕ and α. (b) The same parameters in real space.

and

$$T = 1.19\text{–}1.21 \text{ from equation (9).}$$

To find the position of the circle in stretch space the vertical distance from the horizontal axis must also be known. This can be defined in terms of ϕ and T (see Fig. 2). ϕ is related to β in the following way:

$$\frac{\sin(\beta + \alpha)}{T} = \frac{\sin\phi}{R} \text{ from the sine rule (Fig. 9).}$$

Substitute $\alpha = \beta + \phi$ then after expanding and simplifying this becomes

$$\tan\phi = \frac{R\sin 2\beta}{(T - R\cos 2\beta)}. \qquad (12)$$

For this sample $5° < \beta < 8°$. Therefore from equation (12) and the previously determined values of T and R, $12° < \phi < 19°$. W_m can then be calculated from (10) and (11) which gives a range for W_m of

$$0.35 < W_m < 0.60.$$

GRAPHICAL DETERMINATION OF W_m

The above two methods give a range of possible values for W_m. The range of values can be shown by plotting a number of different Mohr circles. Alternatively for deformation that conserves area the estimates for W_m can be plotted on one diagram using the angle ϕ. The radius and distance from the origin of the Mohr circle, R and T, are defined from the value of the finite strain. It is therefore possible to plot trajectories for the centres of Mohr circles at given values of finite strain for varying W_m (Passchier 1988a). To find the value of W_m a line is drawn from the origin at an angle ϕ to the horizontal axis. This line intersects a curve for the appropriate value of finite strain at a point that corresponds to a unique value of W_m (Fig. 10).

DISCUSSION

Deformation of the veins and the matrix material is associated with very similar values for finite strain. Therefore, both the quartz c-axis fabric and the deformed veins probably developed throughout the period of ductile deformation. However, quartz c-axis fabrics will be reset by dynamic recrystallization so that only the later parts of the deformation history are preserved. The consistent results for W_m using the two different methods indicate therefore that the degree of instantaneous non-coaxiality, W_n, was not strongly time dependent.

The estimates for W_m show that deformation in the metachert deviated substantially from simple shear. The stretch along A_1 can be measured directly from the Mohr circle for F_{ij} and the inverse gives the amount of thinning perpendicular to the flow plane. As an example, values of $R_f = 3.5$, $W_m = 0.5$ imply a thinning of about 400 m for every 1 km original thickness.

Much of the Sanbagawa Belt has undergone penetrative deformation associated with the formation of a prominent stretching lineation oriented roughly parallel to the trend of the belt (Hara *et al.* 1977, 1990, Toriumi 1982, Faure 1985, Wallis & Banno 1990). This deformation can be directly compared to the phase of deformation studied in this sample. The topology of quartz c-axis fabrics and other kinematic indicators suggest deviations from simple shear in higher grade parts of the Sanbagawa Belt (Kojima & Hide 1958, Wallis unpublished). Although these data have not yet been quanti-

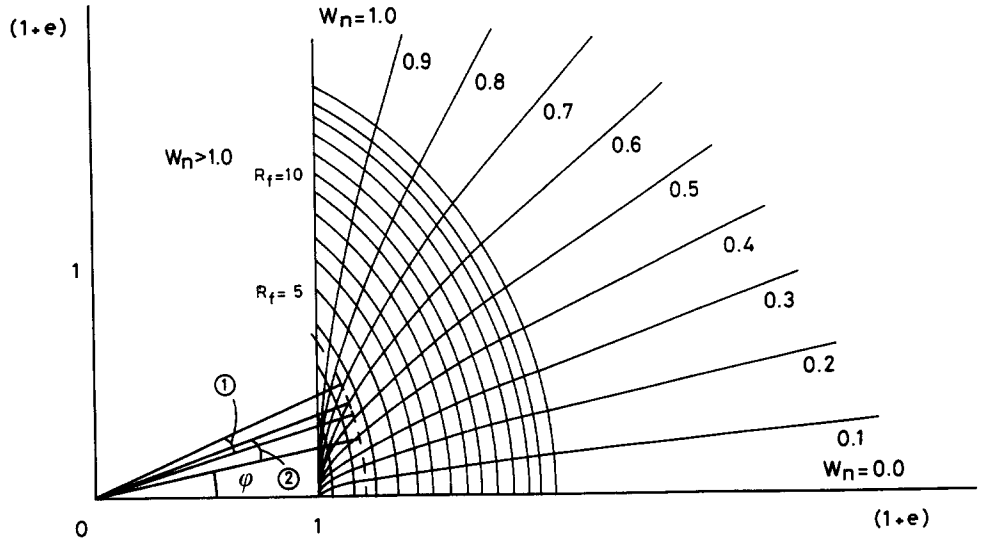

Fig. 10. Graphical representation of the possible centres of Mohr circles in stretch space that arise from equal area progressive steady flow, i.e. $W_n = W_m$, with different vorticity numbers (after Passchier 1988a). A value of W_m can be found from a knowledge of ϕ and R_f. This representation of the parameters of the Mohr circle has the advantage that several estimates can be plotted on the same figure and maximum and minimum estimates for W_m readily identified. Dashed line is for $R_f = 3.5$. ① = the range of estimated W_m from the sets of deformed veins; ② = the range of estimated W_m from the quartz *c*-axis fabric.

fied, they suggest that the main tectonic fabric of the Sanbagawa Belt developed during general non-coaxial shear with $W_m < 1$. This is opposed to the proposition of Faure (1985) that deformation throughout the Sanbagawa Belt was by simple shear. A deformation path associated with $W_m < 1$ causes shortening perpendicular to the flow plane and this could be a significant factor in the exhumation of high *P–T* rocks in this region.

A similar vorticity analysis could be carried out in other areas where there are data on the finite strain and the orientation of certain fixed elements of the flow. Suitable areas might be the Cambrian quartzites of the Moine area in Scotland (Law *et al.* 1984) and the quartz-rich tectonites of the Betics of southern Spain (Platt & Behrmann 1986).

CONCLUSIONS

Deformed metachert is a potentially very useful material for vorticity analyses because it commonly contains features that allow the finite strain to be determined as well as the orientation of certain fixed elements of flow. Sets of deformed veins also allow an estimate of the amount of volume change during deformation. The results from the Sanbagawa Belt suggest that deformation was roughly time constant with a significant departure from simple shear. High-strain deformation of this type could cause significant subvertical shortening and be an important factor in the exhumation of the Sanbagawa Belt.

Acknowledgements—My thanks to Shohei Banno for introducing me to the area. Subir Ghosh and in particular Cees Passchier provided detailed reviews that together with the careful editing of Sue Treagus considerably helped to improve an earlier version of the manuscript. This work was carried out under the tenure of a Royal Society/JSPS fellowship.

REFERENCES

Bell, T. H. & Etheridge, M. A. 1973. Microstructure of mylonites and their descriptive terminology. *Lithos* **6**, 337–348.

Bobyarchick, A. R. 1986. The eigenvalues of steady flow in Mohr space. *Tectonophysics* **122**, 35–51.

Cowan, D. S. 1990. Kinematic analysis of shear zones in sandstone and mudstone of the Shimanto belt, Shikoku, SW Japan. *J. Struct. Geol.* **12**, 431–441.

De Paor, D. G. 1988. R_f/ϕ strain analysis using an orientation net. *J. Struct. Geol.* **10**, 323–333.

Elliott, D. 1972. Deformation paths in structural geology. *Bull. geol. Soc. Am.* **83**, 2621–2638.

Faure, M. 1985. Microtectonic evidence for eastward ductile shear in the Jurassic orogen of SW Japan. *J. Struct. Geol.* **7**, 175–186.

Fisher, N. I., Lewis, T. & Embleton, B. J. J. 1987. *Statistical Analysis of Spherical Data*. Cambridge University Press, Cambridge.

Ghosh, S. K. 1987. Measure of non-coaxiality. *J. Struct. Geol.* **9**, 111–113.

Ghosh, S. K. & Ramberg, H. 1976. Reorientation of inclusions by combination of pure and simple shear. *Tectonophysics* **34**, 1–70.

Hara, I., Hide, K., Takeda, K., Tsukuda, E., Tokuda, M. & Shiota, T. 1977. Tectonic movement in the Sambagawa Belt. In: *The Sambagawa Belt* (edited by Hide, K.). Hiroshima University Press.

Hara, I., Shiota, K., Okamoto, K., Takeda, K., Hayasaka, Y. & Sakurai, Y. 1990. Nappe structure of the Sambagawa Belt. *J. metamorph. Geol.* **8**, 441–456.

Hutton, D. H. W. 1982. A tectonic model for the emplacement of the main Donegal granite, NW Ireland. *J. geol. Soc. Lond.* **139**, 615–631.

Kojima, G. & Hide, K. 1958. Kinematic interpretation of the quartz fabric of triclinic tectonites from Besshi, Central Shikoku. *Japan, J. Fac. Sci., Hiroshima Series* **C2**, 195–226.

Law, R. D., Casey, M. & Knipe, R. J. 1986. Kinematic and tectonic significance of microstructures and crystallographic fabrics within quartz mylonites from Assynt and Eriboll regions of the Moine thrust zone, NW Scotland. *Trans. R. Soc. Edinb.* **77**, 99–125.

Law, R. D., Knipe, R. J. & Dayan, H. 1984. Strain path partitioning within thrust sheets: microstructural and petrofabric evidence from the Moine thrust zone at Loch Eriboll, northwest Scotland. *J. Struct. Geol.* **6**, 477–497.

Law, R. D., Schmid, S. M. & Wheeler, J. 1990. Simple shear deformation and quartz crystallographic fabrics: a possible natural example from the Torridon area of NW Scotland. *J. Struct. Geol.* **12**, 29–45.

Lister, G. S. & Hobbs, B. E. 1980. The simulation of fabric development during plastic deformation and its application to quartzite: the influence of deformation history. *J. Struct. Geol.* **2**, 355–370.

Lister, G. S. & Williams, P. F. 1979. Fabric development in shear zones: theoretical controls and observed phenomena. *J. Struct. Geol.* **6**, 617–638.

Lister, G. S. & Williams, P. F. 1983. The partitioning of deformation in flowing rock masses. *Tectonophysics* **92**, 1–33.

MacKenzie, D. P. 1979. Finite deformation during fluid flow. *Geophys. J. R. astr. Soc.* **58**, 689–715.

Malvern, L. E. 1969. *Introduction to the Mechanics of a Continuous Medium*. Prentice-Hall, Englewood Cliffs, New Jersey.

Means, W. D. 1982. An unfamiliar Mohr circle construction for finite strain. *Tectonophysics* **89**, T1–T6.

Means, W. D. 1983. Application of the Mohr-circle construction to problems of inhomogeneous deformation. *J. Struct. Geol.* **5**, 279–286.

Means, W. D., Hobbs, B. E., Lister, G. S. & Williams, P. F. 1980. Vorticity and non-coaxiality in progressive deformations. *J. Struct. Geol.* **2**, 371–378.

Passchier, C. W. 1986. Flow in natural shear zones—the consequences of spinning flow regimes. *Earth Planet. Sci. Lett.* **77**, 70–80.

Passchier, C. W. 1987a. Efficient use of the velocity gradients tensor in flow modelling. *Tectonophysics* **136**, 159–163.

Passchier, C. W. 1987b. Stable positions of rigid objects in non-coaxial flow—a study in vorticity analysis. *J. Struct. Geol.* **9**, 679–690.

Passchier, C. W. 1988a. Analysis of deformation paths in shear zones. *Geol. Rdsch.* **77**, 309–318.

Passchier, C. W. 1988b. The use of Mohr circles to describe non-coaxial progressive deformation. *Tectonophysics* **149**, 323–338.

Passchier, C. W. 1990a. Reconstruction of deformation and flow parameters from deformed vein sets. *Tectonophysics* **180**, 185–199.

Passchier, C. W. 1990b. A Mohr circle construction to plot the stretch history of material lines. *J. Struct. Geol.* **12**, 513–515.

Passchier, C. W. 1991. The classification of dilatant flow types. *J. Struct. Geol.* **13**, 101–104.

Passchier, C. W. & Urai, J. L. 1988. Vorticity and strain analysis using Mohr diagrams. *J. Struct. Geol.* **10**, 755–763.

Platt, J. P. & Behrmann, J. H. 1986. Structures and fabrics in a crustal-scale shear zone. Betic Cordillera, S. E. Spain. *J. Struct. Geol.* **8**, 15–33.

Ramsay, J. G. & Huber, M. I. 1983. *The Techniques of Modern Structural Geology, Volume* 1: *Strain Analysis*. Academic Press, New York.

Schmid, S. M. & Casey, M. 1986. Complete fabric analysis of some commonly observed quartz *c*-axis patterns. In: *Mineral and Rock Deformation: Laboratory Studies—The Paterson Volume* (edited by Hobbs, B. E. & Heard, H. C.). *Am. Geophys. Un. Geophys. Monogr.* **36**, 263–286.

Talbot, C. J. 1970. The minimum strain ellipsoid using deformed quartz veins. *Tectonophysics* **9**, 46–76.

Toriumi, M. 1982. Strain, stress and uplift. *Tectonics* **1**, 57–76.

Treagus, S. H. 1990. The Mohr diagram for three dimensional reciprocal stretch vs rotation. *J. Struct. Geol.* **12**, 383–395.

Truesdell, C. 1954. *The Kinematics of Vorticity*. Indiana University Press, Bloomington, Indiana.

Vissers, R. L. M. 1989. Asymmetric quartz *c*-axis fabrics and flow vorticity: a study using rotated garnets. *J. Struct. Geol.* **11**, 231–244.

Wallis, S. R. & Banno, S. 1990. The Sambagawa Belt: trends in research. *J. metamorph. Geol.* **8**, 393–399.

Watanabe, T. & Kobayashi, H. 1984. Occurrence of lawsonite in pelitic schists from the Sanbagawa belt, the Asemigawa region, central Shikoku. *J. metamorph. Geol.* **2**, 365–369.

White, S. H. 1976. The effects of strain and microstructure fabrics and deformation mechanisms in quartzite. *Phil. Trans. R. Soc. Lond.* **A283**, 69–86.